Noname manuscript No.
(will be inserted by the editor)

Core-level shift analysis of amorphous $CdTeO_x$ materials

R. Lizárraga · E. Holmström · A. Amézaga · N. Bock · T. Peery · E. Menéndez-Proupin · P. Giannozzi.

February 25, 2010

Abstract We show the importance of considering the detailed local distributions of oxygen atoms around tellurium in $CdTeO_x$ glasses when interpreting X-ray photoemission experiments. We perform first principles calculations of core-level shifts that are used to compute X-ray photo-electron spectra. The core-level shifts are investigated by means of atomic density of states and a structural Voronoi analysis. We find that the dominating effect on the atomic core-level shift of tellurium is charge redistribution due to the oxygen atoms. There is however also a prominent effect from the geometrical arrangement of the oxygen neighbors.

Keywords X-Ray Spectroscopy · Core-level-shifts · first principles calculations, Pacs: 79.60.Ht,71.15.Mb,61.43.Bn,61.43.Dq

R. Lizárraga and E. Holmström
Instituto de Física, Facultad de Ciencias, Universidad Austral de Chile, Casilla 567, Valdivia, Chile
E-mail: raquellizarraga@uach.cl, eholmstrom@uach.cl

A. Amézaga
Instituto de Matematica, Facultad de Ciencias, Universidad Austral de Chile, Casilla 567, Valdivia, Chile
E-mail: amezagahv@gmail.com

N. Bock and T. Peery
Theoretical Division, Los Alamos National Laboratory, Los Alamos, New Mexico 87545, USA
E-mail: nbock@lanl.gov, tpeery@lanl.gov

E. Menéndez-Proupin
Departamento de Física, Facultad de Ciencias, Universidad de Chile, Las Palmeras 3425, 780-0024 Ñuñoa, Santiago, Chile
E-mail: emenendez@uchile.cl

P. Giannozzi
Department of Physics, University of Udine, via delle Scienze 208, I-33100, Udine, Italy and CNR-INFM DEMOCRITOS National Simulation Center, I-34014 Trieste, Italy
E-mail: paolo.giannozzi@uniud.it

1 Introduction

Structural analysis of amorphous materials can be a challenge since the lack of symmetries and infinite range of possible local environments for an element may complicate the interpretation of the experimental data. X-ray photo-electron spectroscopy (XPS) is a widely used experimental technique for extracting information of chemical compositions, local environment effects and the electronic structure of solids. (1) Chemical compositions are the most straightforward information that can be obtained in the analysis of the XPS spectrum by integrating each peak corresponding to each element.

The determination of the different chemical environment of a single element within a material is however more difficult and requires additional information to aid the analysis of the spectral line shapes. In crystals, for instance, X-ray diffraction of the crystal structure can limit the number of parameters in the curve fitting procedure. Hence, more than one experimental technique are needed to interpret and obtain structural information of solids. Amorphous materials complicate interpretation because of their lack of crystalline order and subsequent local environmental disorder.

Computer simulations can provide valuable information and an efficient way to analyze experimental XPS data in solids. For amorphous materials, the random structure can be modeled, for example, by means molecular dynamics (MD) simulations and the spectrum accurately calculated from first principles. One of the advantages of this approach is that the correlation between local environments and spectral peak shapes and positions can readily be accessed since the contributions to the spectrum from individual atoms are known.

Recently, this procedure has successfully been applied to amorphous $CdTeO_x$ ($x = 0.2, 1, 2, 3$) (2). In that work, the tellurium electron relative core-level energies were calculated by means of density functional theory (DFT) (3; 4) and then used to compute the XPS spectra. The results corroborated the existence of a correlation between the magnitudes of two tellurium peaks in the XPS spectrum (5; 6; 7; 8; 9) and the number of oxygen atoms in close chemical proximity of the tellurium sites. As yet, however, no quantitative analysis of the atomic environments that built the individual peaks has been presented.

In the present paper, we describe the tellurium local environments that compose each peak in the XPS spectra. We show that some tellurium atoms with the same number of oxygen neighbors have local environments with different geometries that do not contribute to the same peak in the spectrum. We analyze the structures and charge redistribution by means of structure factors, density of states and Voronoi volumes for the amorphous CdTeO oxides.

2 Theory

2.1 XPS spectra

Experimentally the initial photoemission state consists of a sample in its ground state plus an X-ray photon, and the final state is a sample with a core hole (one electron missing in a deep core-level) plus an electron leaving the crystal (photo-electron). The binding energy is defined as $E_B = E_f^{N-1} - E_i^N$ where E_i^N is the energy of the initial state with N electrons and E_f^{N-1} is the energy of the final state with one missing

electron. The photo-electron binding energy is measured in an XPS experiment as (10)

$$E_B = \hbar\omega - E_{\rm kin} + E_{\rm ref}, \tag{1}$$

where $\hbar\omega$ is the X-ray photon energy, $E_{\rm kin}$ is the kinetic energy of the photo-electron measured with a detector, and $E_{\rm ref}$ is a reference that may be the common Fermi level of the sample and the detector in the case of metallic samples. The core-level shift (CLS) can then be defined as the difference in binding energy between different atomic sites in a material.

The accurate calculation of absolute binding energies is a difficult theoretical problem, but, energy differences are generally well described by density functional theory (DFT) methods (3; 4). In particular, for amorphous CdTeO oxides, the binding energy difference can be expressed as

$$\Delta E_B = E(CdTe_{1-y}Te^*_yO_x) - E(CdTeO_x), \tag{2}$$

where $E(CdTe_{1-y}Te^*_yO_x)$ is the total energy of the supercell with a concentration of core-ionized atoms y equal to one over the number of Te atoms in the supercell. Substitution of Te by Te^* (the excited atom) at different sites provides the site-dependent CLS.

In the pseudopotential method we are using in this study we cannot directly ionize a core electron. A way around this problem is to represent the excited Te^* atom by a new pseudopotential (11) that has a missing core electron, or simply approximate Te^* with the addition of a proton to the nucleus, i.e., the next element of the periodic table.(12) The latter approximation is called the $Z + 1$ approximation.

The site dependent binding energy differences are smeared and then summed up to form the continuous line of the XPS spectrum. The result is a theoretical XPS spectrum where the energy scale is not absolute.

3 Computational Details

Our first principles, self-consistent electronic structure calculations were performed by means of DFT using the pseudopotential method implemented in the Vienna Ab-initio Simulation Package (VASP) (13) and Quantum ESPRESSO (QE) (14) code. The exchange correlation energy was calculated employing the generalized gradient approximation with the Perdew, Burke, and Ernzerhof functional.(15)

The electronic states in the DFT calculation were expanded using a plane wave basis set with a cutoff of 400 eV for VASP and 530 eV for QE calculations. We used the projector augmented wave potentials with $5s$ and $5p$ valence states for Te, $4d$ and $5s$ for Cd and $2s$, $2p$ for O. The number of k-points was carefully optimized in order to achieve energy convergence, giving a $2\times2\times2$ Monkhorst-Pack Brillouin zone sampling.

We have checked the reliability of the Z+1 approximation in our system, using the QE code and a Te* pseudopotential with a missing core electron(2).

In the present investigation, we utilized structural models for amorphous $CdTeO_x$ obtained by MD simulations [1]. The MD procedure used to produce the amorphous structures was carefully described in Ref.(16). The supercell sizes for $CdTeO_x$ were

[1] See EPAPS Document No. E-PRBMDO-78-102845 for the atomic coordinates in XYZ format. For more information on EPAPS, see http://www.aip.org/pubservs/epaps.html.

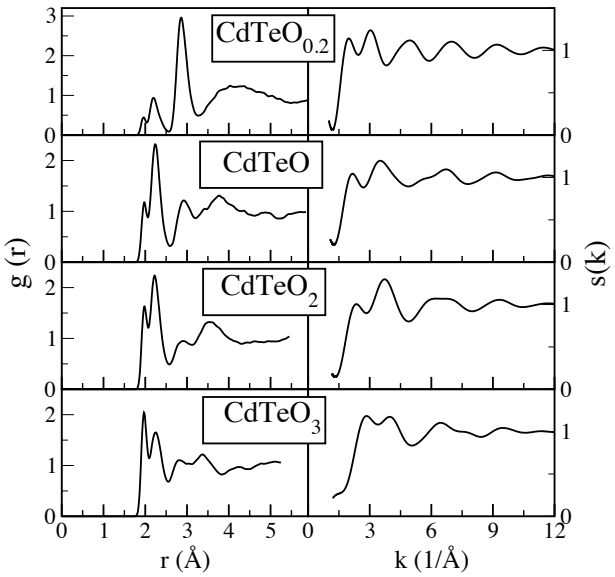

Fig. 1 The calculated pair distribution function $g(r)$ (left panel) and the static structure factor $S(k)$ (right panel) for the $CdTeO_{0.2}$, CdTeO, $CdTeO_2$ and $CdTeO_3$ structures.

adjusted by linear interpolation to fit the experimental densities of the crystalline materials CdTe and $CdTeO_3$, where ρ(CdTe)= 5.85 g/cm^3 and $\rho(CdTeO_3)$= 6.416 g/cm^3. The total number of atoms in each supercell was 66, 72, 76, and 80 for x =0.2, 1, 2, and 3 respectively. These structures were thoroughly characterized using several statistical properties, such as the pair distribution functions, angle distribution functions and coordination histograms. From the analysis in Ref. (16) it was found that the CdTeO and $CdTeO_2$ compounds present more chemical and topological disorder than $CdTeO_{0.2}$ and $CdTeO_3$.

4 Results and Discussion

4.1 Statistical Structural Analysis

In the left panel of Fig.1 we show the calculated total pair distribution functions $g(r)$ for $CdTeO_x$ with $x = 0.2, 1, 2, 3$. The distance to the first minima in the $g(r)$ determines the radius of a spherical shell containing nearest neighbors. For all compositions x, we observe that the first peak is split into two peaks, corresponding to the distance between tellurium and oxygen nearest neighbors (approximately 1.97 Å) and between cadmium and oxygen neighbors (approximately 2.23 Å).

Since the static structure factor $S(k)$ is directly accessible to neutron or X-ray scattering experiments we show them for the amorphous compounds in the right panel of Fig.1. All of them have two peaks below 4.5 Å^{-1}, the second one being slightly higher than the first one except for $x = 3$, where the two peaks have almost identical height. This is due to the higher oxygen content of $CdTeO_3$, as the first peak in $S(k)$ is determined by O-O and Cd-O contributions.

4.2 Local Structural Analysis, Characteristic Environments

The oxygen geometries in the local environments of the Te atoms were closely inspected for each supercell. In our amorphous structures each atomic environment is unique, but within a small margin of error, we were able to identify some idealized characteristic structures. The Te atoms with one oxygen neighbor are all well represented by a Te-O dimer. The Te atoms with two oxygen neighbors are represented by a O-Te-O molecule with bond angle 90°. In the case of three-coordinated Te, we find one "planar" geometry and one "pyramidal" geometry. The "planar" geometry is T-shaped with the Te in the center and all bond angles 90° (oxygen in the $+x$, $-x$, and $+y$ directions). The "pyramidal" geometry is a pyramid with the Te at the top and the oxygen atoms at the base, constructed with all bond angles 90° (oxygen in the $+x$, $+y$, and $+z$ directions). The four-coordinated Te atoms have oxygen in the $+x$, $-x$, $+y$, and $+z$ directions, and the five-coordinated Te have oxygen in the $+x$, $-x$, $+y$, $-y$, and $+z$ directions. All these characteristic structures are shown in Figs. 2-5. In the identification of these structures, only Te-O bond distances within the first peak of the pair distribution function were considered. The spread in bond angles is about 5°.

4.3 Local Environment Effects in Spectral Peaks

In order to investigate the effects of the local atomic environments on the XPS spectra, we show the site-dependent CLS of each characteristic structures in Figs. 2-5.

In these figures the CLS of each local Te environment is indicated by vertical bars and the typical geometries in which these local environments are found are indicated by arrows. The height of each bar represents the number of oxygen neighbors of the particular Te site. In counting the number of oxygen neighbors we employed a radial cutoff of 2.32 Å, which is the distance of the first minimum of the partial Te-O radial distribution function of our amorphous structures.(16) To compute the XPS spectrum, the calculated electron core levels were represented by normalized Gaussians of width 0.5 eV which were then summed up to form the dashed line of the spectrum.

Two spectral peaks are seen in all materials except $CdTeO_3$ which has only one. When discussing theses amorphous spectra in the literature,(7; 17; 5) the peak to the right has often been assigned to Te bound to Cd atoms, while the peak to the left has been assigned to Te bound to O atoms. Figs. 2-5 demonstrate, however, that each peak has associated tellurium atoms with different local environments. Each peak therefore contains contributions from one or more tellurium atoms with a different number of oxygen neighbors. In particular, we can see that the right peak is mainly composed of Te atoms with 0 and 1 oxygen nearest neighbors and that the left peak is mainly Te atoms with 3-5 oxygen neighbors. The Te atoms that have 2 oxygen neighbors tend to experience varying core-level shifts and cannot be assigned to any of the two spectral peaks only.

Moreover, a close inspection of the Te local environments $CdTeO_2$ in Fig. 4 shows that tellurium atoms with three oxygen nearest neighbors experience different CLS because they are arranged in different geometries. The Te atoms in the planar configuration have a CLS that is about 1 eV lower than the Te atoms in the pyramidal configuration and thus contribute to different peaks in the total XPS spectrum. This case cannot be explained by considering the number of oxygen neighbors alone, but must be attributed to the strong directional bonding of the p orbitals.

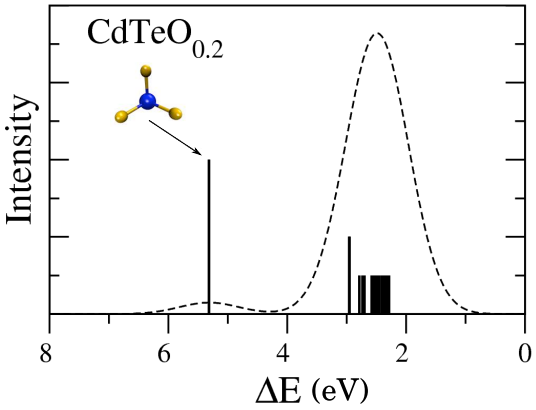

Fig. 2 (Color online) The calculated tellurium XPS spectrum is shown for $CdTeO_{0.2}$. The bars indicate the tellurium energy shifts and the height of the bars denote the number of oxygen neighbors which was calculated within a cutoff radius of 2.32 Å. Typical Te environments are depicted as well, where the blue balls are Te atoms and the yellow ones represent oxygen.

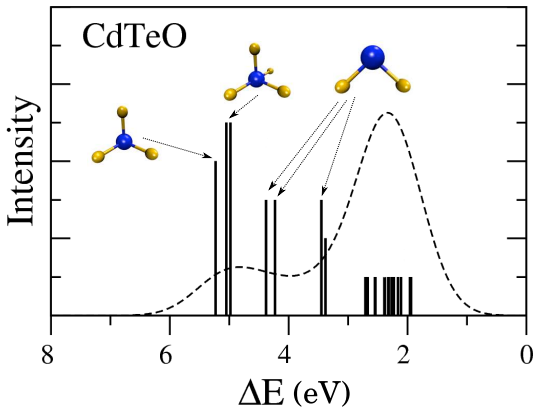

Fig. 3 (Color online) The calculated tellurium XPS spectrum is presented for CdTeO. The bars indicate the tellurium energy shifts and the height of the bars denote the number of oxygen neighbors which was calculated within a cutoff radius of 2.32 Å. Typical Te environments are depicted as well, where the blue balls are Te atoms and the yellow represent oxygen.

In general, the trend is that the binding energy increases as a function of the number of oxygen atoms around Te, but the conclusion is also that both peaks contain signals from Te atoms with at least one oxygen atom in its local environment.

4.3.1 Tellurium Density Of States

The atomic density of states (DOS) for each tellurium atom in the cell is displayed in Fig. 6. For each structure, the DOS is arranged from top to bottom in order of increasing binding energy so that the top DOS corresponds to the Te atom with the lowest binding energy. In both CdTeO and $CdTeO_2$ we observe a distinctive peak around -6 eV in the DOS at the bottom that disappears as the binding energy becomes lower. At around the DOS where this peak disappears another peak forms close to the Fermi level and it

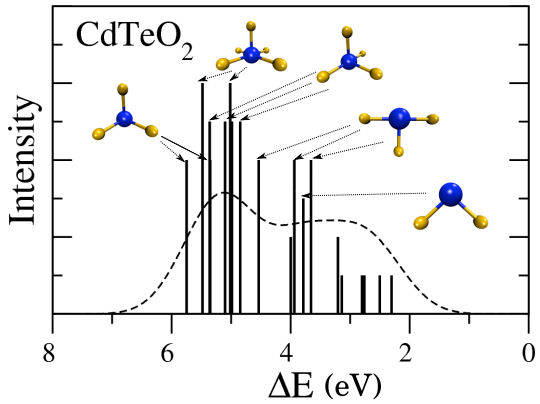

Fig. 4 (Color online) The calculated tellurium XPS spectrum is displayed for $CdTeO_2$. The bars indicate the tellurium energy shifts and the height of the bars denote the number of oxygen neighbors which was calculated within a cutoff radius of 2.32 Å. Typical Te environments are depicted as well, where the blue balls are Te atoms and the yellow ones represent oxygen.

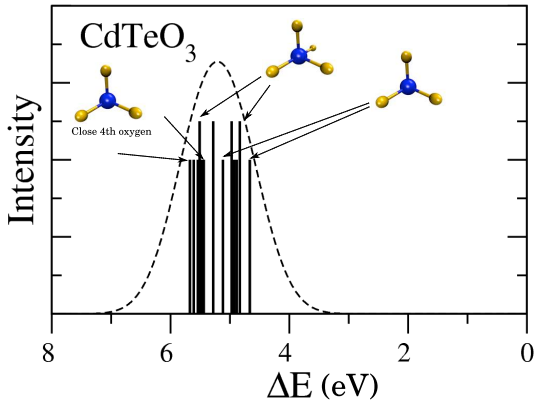

Fig. 5 (Color online) The calculated tellurium XPS spectrum is shown for $CdTeO_3$. The bars indicate the tellurium energy shifts and the height of the bars denote the number of oxygen neighbors which was calculated within a cutoff radius of 2.32 Å. Typical Te environments are depicted as well, where the blue balls are Te atoms and the yellow represent oxygen. In this case, the characterization of the three-coordinated Te sites was difficult to perform due to the large amount of oxygen present. The ambiguous characteristic environments had a close 4th oxygen atom that was still outside the cutoff radius and they are marked in the figure.

remains all the way up to the top DOS. $CdTeO_{0.2}$ has a peak close to the Fermi level for all Te atoms and while it is still possible to distinguish this peak in $CdTeO_3$, it is less prominent. These observations indicate big differences in charge redistributions between Te sites in the materials.

To quantify this variation we plotted the correlation between the center of gravity of each DOS and the site-dependent binding energy differences in Fig.7. The DOS center of gravity for CdTeO and $CdTeO_2$ varies appreciably and shows a clear correlation with the binding energy. The fact that the binding energy becomes larger when the DOS center of gravity moves towards lower energies indicates a charge transfer process.

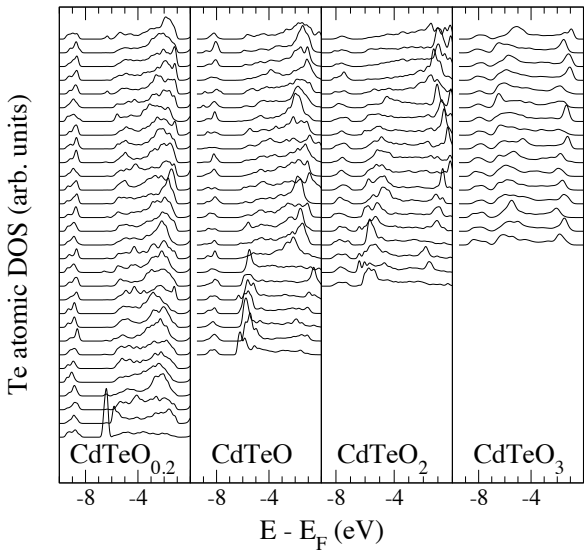

Fig. 6 Density of states for each tellurium atom in the cell for $CdTeO_{0.2}$, CdTeO, $CdTeO_2$ and $CdTeO_3$. The Fermi level is located at 0 eV. The order is so that the DOS of the Te atom with the lowest binding energy is at the top.

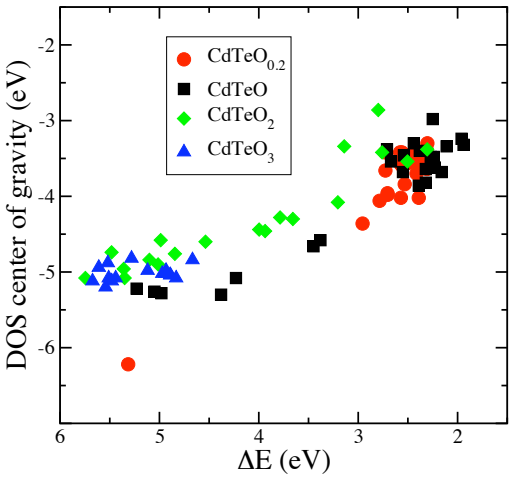

Fig. 7 (Color online) Center of gravity of the DOS for each tellurium atom displayed as a function of the site dependent core-level shift for $CdTeO_{0.2}$, CdTeO, $CdTeO_2$ and $CdTeO_3$.

The situation is somewhat different for $CdTeO_{0.2}$ and $CdTeO_3$ where the DOS center of gravity does not change much. This indicates that all Te sites have similar local environments, and hence experience similar amounts of charge transfer.

4.3.2 Local Cell Volumes

We have also investigated the effects of local environment volumes of the Te atoms. This was done by means of the Voronoi polyhedron volumes. A Voronoi polyhedron

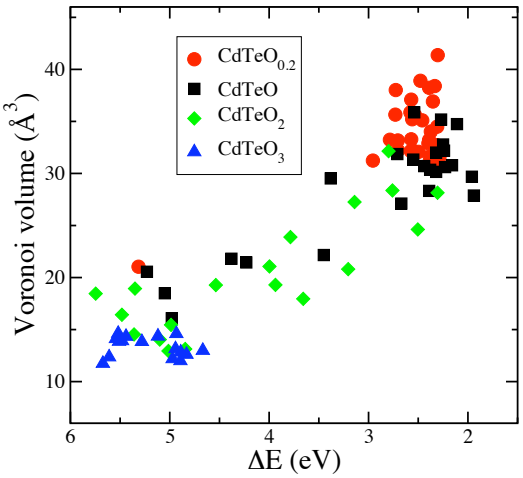

Fig. 8 (Color online) Voronoi volume for $CdTeO_{0.2}$, CdTeO, $CdTeO_2$ and $CdTeO_3$ shown as a function of site dependent core-level shift.

is constructed by bisecting planes the same way as in a normal Wigner-Seitz cell construction, with the difference that the structure consists of irregularly spaced atoms. This results in irregular polyhedra surrounding each atom in the structure whose volume represents the local space available to the atom. We encounter a strong correlation between these Voronoi volumes and the site dependent CLS. The results can be seen in Fig.8. In the figure we can see that Te atoms in $CdTeO_{0.2}$ with larger Voronoi volumes have lower binding energy. There is one Te atom with a small Voronoi volume that has high binding energy which corresponds to the three coordinated Te atom in the left peak in Fig.2. For all the systems, there is a clear correlation between the Voronoi volume and the binding energy over the whole range of local volumes and CLS.

5 Conclusions

We have performed a quantification of the local Te environments in terms of detailed geometries in amorphous CdTeO materials with varying oxygen content. We have shown that the most important effect on the Te CLS is charge redistribution of the valence electrons due to oxygen proximity but in the case of $CdTeO_2$ there is a prominent effect of directional bonding on the site-dependent Te CLS as well. The charge redistribution is manifested in a change in the center of gravity of the site-dependent Te DOS. The short bond lengths in the Te-O bonds results in a strong correlation between the Te Voronoi cell volumes and the site-dependent Te CLS. We believe that our results show the usefulness of first principles calculations in the characterization of important amorphous oxides such as Al_2O_3, TiO, etc.

6 Acknowledgments

This work was supported by DID (UACH) grant S-2008-42 and Anillo ACT/ADI-24 Chile grant. EH and RL also acknowledge support from FONDECYT projects 11070115 and 11080259, DID (UACH) grants SR-2008-0 and S-2008-51.

References

1. F. de Groot, A. Kotani (eds.), *Core Level Spectroscopy of Solids*, vol. 6 (CRC Press, London, 2008)
2. A. Amézaga, E. Holmström, R. Lizárraga, E. Menéndez-Proupin, P. Bartolo-Pérez, P. Giannozzi, Phys. Rev. B **71**, 014210 (2010)
3. P. Hohenberg, W. Kohn, Phys. Rev. **136**, B864 (1964)
4. W. Kohn, L. Sham, Phys. Rev. **140**, A1133 (1965)
5. P. Bartolo-Pérez, R.C. Rodríguez, F. Caballero-Briones, W. Cauich, J.L. Peña, M.H. Farias, Surf. Coat. Technol. **155**, 16 (2002)
6. P. Bartolo-Pérez, J.L. Peña, M.H. Farias, Sup. Vac. **8**, 59 (1999)
7. A. Zapata-Navarro, M. Zapata-Torres, V. Sosa, P. Bartolo-Pérez, J.L. Peña, J. Vac. Sci. Technol. A **12**, 714 (1994)
8. A. Zapata-Navarro, P. Bartolo-Pérez, M. Zapata-Torres, R. Castro-Rodríguez, J.L. Peña, J. Vac. Sci. Technol. A **15**, 2537 (1997)
9. F. Caballero-Briones, A.I. Oliva, P. Bartolo-Pérez, A. Zapata-Navarro, J.L. Peña, Thin Solid Films **516**, 8289 (2008)
10. S. Hüfner, *Photoelectron spectroscopy: principles and applications*, 2nd edn. (Springer, Berlin, 1995)
11. E. Pehlke, M. Scheffler, Phys. Rev. Lett. **71**(14), 2338 (1993). DOI 10.1103/PhysRevLett.71.2338
12. B. Johansson, N. Martensson, Phys. Rev. B **21**(10), 4427 (1980)
13. G. Kresse, J. Furthmüller, Phys. Rev. B **54**, 11169 (1996)
14. P. Giannozzi, S. Baroni, N. Bonini, M. Calandra, R. Car, C. Cavazzoni, D. Ceresoli, G.L. Chiarotti, M. Cococcioni, I. Dabo, et al., J. Phys. Condens. Matter **21**, 395502 (2009)
15. J.P. Perdew, K. Burke, M. Ernzerhof, Phys. Rev. Lett. **77**, 3865 (1996)
16. E. Menéndez-Proupin, P. Giannozzi, J. Peralta, G. Gutiérrez, Phys. Rev. B **79**(1), 014205 (2009)
17. M.Y. El Azhari, M. Azizan, A. Benouna, A. Outzourhit, E. Ameziane, M. Brunel, Thin Solid Films **295**, 131 (1997)